

# CFD Analysis of the Aerodynamic Effects of the Pantograph Covering Structure on WAG-12 train

Anant *Vidyarathi*<sup>1</sup>, Rohit Sharma<sup>1\*</sup>, and Badal Singh<sup>1</sup>

<sup>1</sup>School of Mechanical Engineering, VIT Bhopal University, Sehore, Madhya Pradesh-466114, India

**Abstract.** Pantographs on high-speed trains significantly impact aerodynamic performance, contributing to drag, turbulence, and energy loss. While prior studies address train aerodynamics broadly, limited research has focused on optimizing pantograph covering structures. This study addresses that gap by evaluating five pantograph fairing designs on the WAG-12 locomotive using CFD simulations. The models were developed in SolidWorks and Fusion 360 and analyzed in ANSYS Fluent under steady state conditions using the SST  $k-\omega$  turbulence model. Key aerodynamic metrics - drag and lift coefficients were compared at highest speed of 120 km/h. Results indicate that Design 3, featuring a 35° inclined fairing with inward curvature, yielded the lowest drag ( $C_d = 0.2881$ ) and lift ( $C_l = 0.062$ ) values, this model was further tested at varying speeds (55 & 150 km/h). Design 3 maintained superior performance across all test speeds. These findings offer practical implications for enhancing train efficiency and stability through aerodynamic refinement of pantograph structures.

## 1 Introduction

Without question, aerodynamic optimization plays a major role in the functionalities of high-speed rail systems. As such, they contribute to energy savings, increase comfort levels for the passengers, and ensure stability of the system during operation. One of the chief causes of aerodynamic drag in high-speed vehicles is the pantograph, which is a device fixed on the roof of a vehicle that is meant to supply electrical power from overhead lines. In fact, the complex shape and the location of the pantograph disrupt the flow of air to a great extent, thus leading to quite high values of drag, flow separation, and turbulence at high speeds [1-2]. Generally, most research has focused on the overall train aerodynamics, but the specific influence of the covering structure for a pantograph is less studied. Liu et al. [3] were able to prove that providing a covering structure on the pantograph sinking platform is able to reduce drag and improve its flow behavior [3]. Another set of literature also focused on the design, placement, and sinking height of a pantograph and their influence on the aerodynamic forces and properties of the flow [2, 4]. This work aims at the research gaps through a presentation of various covering configurations for the pantograph and their influence on WAG-12 locomotive aerodynamics. An attempt is made to determine the most feasible fairing configuration which reduces the drag and lift forces for the locomotive using CFD

---

\* Corresponding author: [rohit.sharma@vitbhopal.ac.in](mailto:rohit.sharma@vitbhopal.ac.in)

simulations. This shall definitely help in enhancing the performance and durability of the high-speed rail system.

## 2 Literature review

Previous studies focused on the role of pantograph structures in aerodynamic drag and flow disruption. Liu et al. [3] demonstrated that covering the structure on pantograph sinking platforms can mitigate drag and turbulence. Xiao et al. [4] demonstrated that the optimization of the sinking height reduces unsteady aerodynamic forces, which enhances stability. Zhang et al. [1] and Zhang & Yang [2] emphasized that the positioning and exposed geometry of a pantograph are crucial for vortex generation and drag.

### 2.1 Noise Emission and Vibration

Pantographs also contribute to aerodynamic noise, particularly at high speeds. The researchers [7-10] found that noise resulting from air-pantograph interaction surpasses rolling noise, stressing the importance of aerodynamic refinement in noise control.

### 2.2 Design Optimization and Drag Reduction

Aerodynamic enhancements for high-speed trains have been the subject of numerous studies, with an emphasis on lowering drag and flow separation around critical components. To reduce wake turbulence and increase overall aerodynamic efficiency, for example, sinking platforms combined with streamlined fairings have been suggested as shown in Figure 1. The addition of streamlined fairings dramatically lowers the train drag coefficient ( $C_d$ ), with reductions of up to 4.30% noted at higher train heights, according to a numerical research on the influence of pantograph fairing on aerodynamic performance at different train heights [11] (see Figure 2).

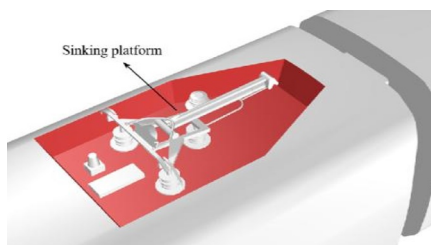


Fig. 1. Sinking platform [3].

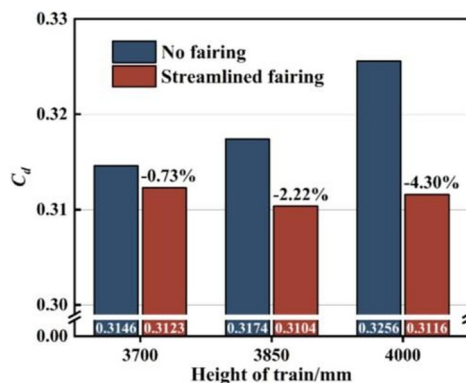


Fig. 2. Variation in train drag coefficient [11].

The comparative analysis of pantograph fairings (3D models of fairing as shown in Figure. 3) indicates that the Type A fairing significantly obstructs the airflow, leading to higher pressure build up and increased aerodynamic drag, making it the least efficient design. On the other hand, the Type B fairing promotes smoother airflow with reduced flow separation and pressure concentration [6]. It was demonstrated by Wu et al. [6] that streamlined pantograph fairings increase energy efficiency and decrease drag. The foundational work by Raghunathan et al. [5] laid the basis for aerodynamic research on high-speed trains, advocating for integrated design solutions.



**Fig. 3.** 3D Models of fairings [6].

Studies on high-speed train aerodynamics have shown that covering the elevated pantograph with streamlined fairings may significantly reduce drag. Table 1 (derived from [3]) shows that the middle car had the greatest drag reduction (28.14%), which contributed to a 5.58% drop in train Cd. Minor decreases were detected for the head car (0.47%) and pantograph (0.52%), but the tail car increased by -22.08%, indicating component-specific aerodynamic interactions that warrant further optimization.

**Table 1.** Aerodynamic drag ( $C_d$ ) for uncovered lifted & covered lifted pantograph [3].

Parts	UL	CL	Change rate
Head car	0.1464	0.1457	0.47%
Middle car	0.1234	0.0887	<b>28.14%</b>
Pantograph	0.0227	0.0226	0.52%
Tail car	0.0694	0.0847	<b>-22.08%</b>
Total	0.3619	0.3417	5.58%

### 2.3 Technical Specifications of WAG-12 train and pantograph

The WAG-12 handbook [12] and RDSO specifications [13] provide operational parameters and mechanical constraints, essential for realistic modeling and ensuring simulation reliability.

## 3 Numerical Setup & Governing Equations

Aerodynamic analysis of five different fairing designs was carried out with ANSYS Fluent. The flow conditions were steady state and incompressible. The SST  $k-\omega$  turbulence model [3, 14-15] was chosen for its high accuracy in the near-wall region and capability of handling flows with adverse pressure gradients. At the inlet, velocity was 120 km/h (33.33 m/s), and

a pressure outlet was set to 0 Pa. The size of the computational domain was determined by 1.5 times the length and 2 times the width of the train model to allow sufficient space for flow development. The body of the train and the pantograph were assumed to be a single solid wall with no-slip conditions, and air was considered as the working fluid with density  $\rho = 1.225 \text{ kg/m}^3$  and dynamic viscosity  $\mu = 1.7894 \times 10^{-5} \text{ Pa}\cdot\text{s}$ . A tetrahedral mesh with inflation layers was used to capture the boundary layer effects. The mesh quality was confirmed by performing skewness and aspect-ratio checks, and that there were no poor elements in the high-gradient regions.

### 3.1 Continuity Equation (Mass Conservation)

$$\nabla \cdot (\rho \mathbf{u}) = 0 \quad (1)$$

$\rho$ : Fluid density ( $\text{kg/m}^3$ ),  $\mathbf{u}$ : Velocity vector ( $\text{m/s}$ ). This equation describes conservation of mass in the fluid domain.

### 3.2 Momentum Equation (Navier-Stokes Equation)

$$\rho(\mathbf{u} \cdot \nabla)\mathbf{u} = -\nabla p + \nabla \cdot \boldsymbol{\tau} + \rho \mathbf{g} \quad (2)$$

$p$ : Pressure (Pa),  $\boldsymbol{\tau}$ : Stress tensor,  $\mathbf{g}$ : Gravitational acceleration vector. This equation represents Newton's second law applied to fluid motion.

### 3.3 SST k-omega Turbulence Model Equations

This model has: k-equation (turbulent kinetic energy),  $\omega$ -equation (specific dissipation rate), this is suitable for near-wall treatment and high adverse pressure gradient flows.

The equation for turbulent kinetic energy ( $k$ ) and specific dissipation rate ( $\omega$ ) is:

$$\mathbf{u} \cdot \nabla k = P_k - \beta * \rho k \omega + \nabla \cdot [(\mu + \sigma k \mu_t) \nabla k] \quad (3)$$

$$\mathbf{u} \cdot \nabla \omega = \frac{\alpha \omega P_k}{k} - \beta \rho \omega^2 + \nabla \cdot [(\mu + \sigma \omega \mu_t) \nabla \omega] + 2(1 - F_1) \rho \sigma \omega^2 (\nabla k \cdot \nabla \omega) / \omega \quad (4)$$

where,  $k$  = Turbulent kinetic energy [ $\text{m}^2/\text{s}^2$ ],  $\omega$  = Specific dissipation rate [ $1/\text{s}$ ],  $P_k$  = Production of turbulent kinetic energy,  $\mu_t$  = Eddy (turbulent) viscosity [ $\text{Pa}\cdot\text{s}$ ],  $\alpha$ ,  $\beta$ ,  $\sigma k$ ,  $\sigma \omega$ ,  $\sigma \omega^2$ : Model constants,  $F_1$ : Blending function to transition between models.

### 3.4 Coefficients Calculated

**Drag Coefficient ( $C_d$ ):**  $C_d = F_d / (0.5 * \rho * V^2 * A)$  (5)

**Lift Coefficient ( $C_l$ ):**  $C_l = F_l / (0.5 * \rho * V^2 * A)$  (6)

where,  $F_d$  = Drag force (N),  $V$  = Free stream velocity (m/s). This indicates resistance offered to motion in the direction of flow.  $F_l$  = Lift force (N), Positive  $C_l$  indicates upward lift; negative indicates downward force.

## 4. Analysis and Results

In the present study, five distinct streamlined CAD models of a single WAG-12 train car equipped with a pantograph were created for aerodynamic simulation, as shown in Figures 4–8. These configurations comprise four fairing designs with varying inclination angles and end curvatures (Designs 1–4), a step-up design (Design 5), and a baseline uncovered train car model (Figure 9).

### 4.1 Geometry preparation

Design 1 has a  $30^\circ$  inclined fairing with a flat end (Figure 4), Design 2 has a  $35^\circ$  outward curvature at the end (Figure 5), Design 3 has a  $35^\circ$  inward curvature (Figure 6), Design 4 has a  $45^\circ$  inclination with flat end (Figure 7), and Design 5 has a step-up profile with  $35^\circ$  inclination (Figure 8). These geometric variations were specifically designed to assess their effectiveness in reducing flow separation, suppressing wake turbulence, and minimizing aerodynamic drag caused by the pantograph sinking platform on high-speed train configurations.

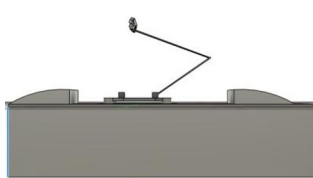


**Fig. 4.** Design 1, Fairing  $30^\circ$  Inclined, with flat end.

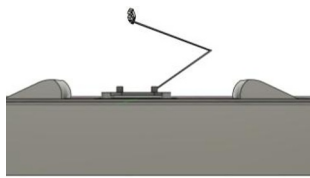


**Fig. 5.** Design 2, Fairing  $35^\circ$  Inclined, with outward curvature at end.

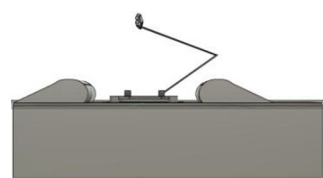


**Fig. 6.** Design 3, Fairing  $35^\circ$  inclined, with inward curvature at the end.

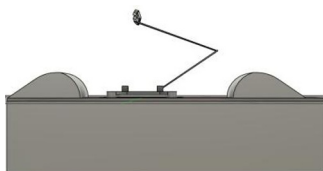


**Fig. 7.** Design 4, Fairing  $45^\circ$  inclined, with flat end.

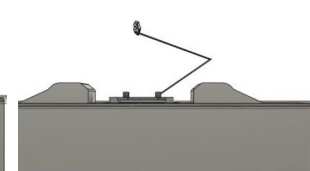


**Fig. 8.** Design 5, Step up design, Fairing  $35^\circ$  inclined with flat end.

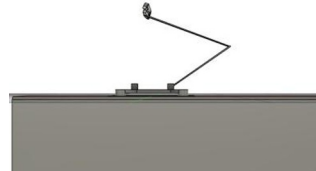


**Fig. 9.** Uncovered train car design.

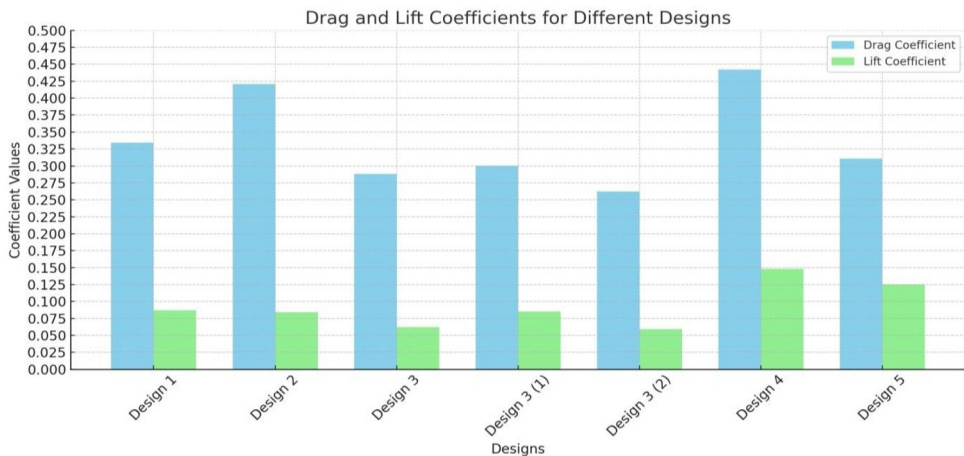
### 4.2 CFD analysis in ANSYS fluent

CFD simulations were conducted in ANSYS Fluent to analyze the aerodynamic performance of the WAG-12 train car with various pantograph fairing designs. The computational domain was generated with a length of  $1.5\times$  and width of  $2\times$  the train model, utilizing Boolean subtraction for precise boundary representation. To account for boundary layer effects, a tetrahedral mesh with inflation layers was used. The SST  $k-\omega$  turbulence model was used to simulate steady incompressible flow conditions with an input velocity of 120 km/h. Drag coefficient ( $C_d$ ) and lift coefficient ( $C_l$ ) values were computed for the uncovered baseline and the five streamlined designs (Table 2 and Figure 10).

**Table 2.** Drag and Lift Coefficients at 120 km/hr.

Design no.	Drag Coefficient ( $C_d$ )	Lift Coefficient ( $C_l$ )
Uncovered (see Figure 9)	0.5923	0.188
Design 1	0.3341	0.087
Design 2	0.4210	0.084
Design 3	0.2881	0.062
	0.3001 (For design 3(1) - At 150km/hr)	0.085 (For design 3(1) - At 150km/hr)
	0.2624 (For design 3(2) - At 55km/hr)	0.059 (For design 3(2) - At 55km/hr)
Design 4	0.4421	0.148
Design 5	0.3105	0.125

The results in Table 2 and Figure 10 demonstrate that the incorporation of streamlined fairings significantly reduces aerodynamic drag compared to the uncovered pantograph configuration ( $C_d = 0.5923$ ). Among the designs, Design 3 ( $35^\circ$  inward-curved fairing) achieves the lowest drag coefficient ( $C_d = 0.2881$ ), representing a substantial improvement over the baseline. Design 5 (step-up fairing) and Design 2 ( $35^\circ$  outward-curved fairing) also show notable drag reductions ( $C_d = 0.3105$  and  $0.4210$ , respectively), while Design 1 ( $30^\circ$  flat-end) and Design 4 ( $45^\circ$  flat-end) yield moderate improvements. Lift coefficients remain relatively low across all designs, with minor variations indicating limited impact on vertical forces. These findings confirm that optimized fairing geometry, particularly inward curvature and appropriate inclination angles, effectively minimizes flow separation and drag around the pantograph sinking platform, enhancing the overall aerodynamic efficiency of high-speed trains.

**Fig. 10.** Comparison of drag coefficient ( $C_d$ ) and lift coefficient ( $C_l$ ) for various designs.

### 4.3 Post processing and streamline analysis

The free-stream airflow moves from left to right across the train model, reaching speeds of up to 33.33 m/s. The creation of recirculation zones and vortex formations highlights the train's blunt-body character [5]. Flow separation is significant around the pantograph in most designs, with distinct vortices developing around its base. However, Design 3 has much smoother streamlines around the fairing, which successfully reduces flow separation and wake turbulence [9]. To go deeper into this behavior, more simulations of Design 3 at various speeds, labeled as 3(1) and 3(2), were run. These findings demonstrate the higher aerodynamic efficiency of the inward-curved fairing structure in suppressing unfavorable flow characteristics when compared to alternative designs.

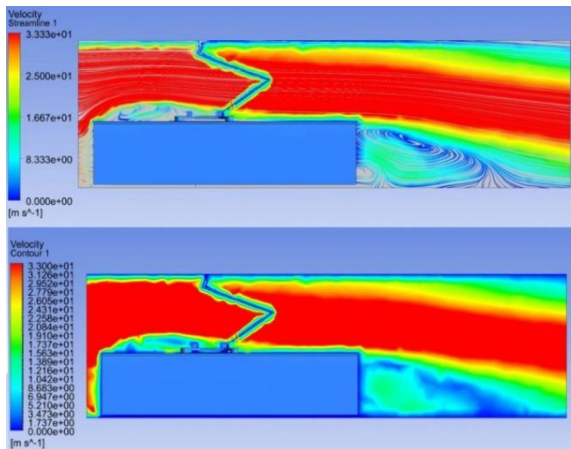


**Fig. 11.** Uncovered train car design.

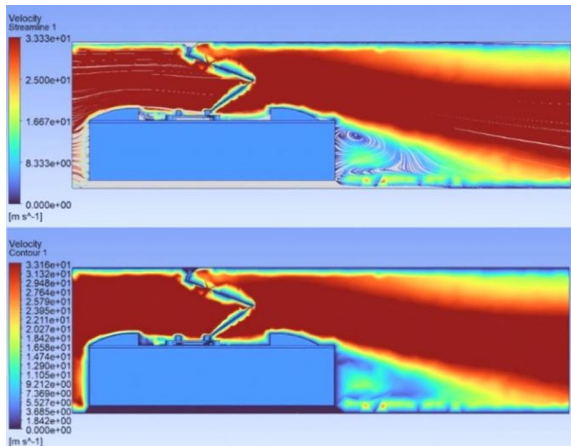


**Fig. 12.** Design 1, Fairing 30° inclined with flat end.

The exposed configuration shows low aerodynamic performance (see Figure 11), which can be understood from the drastic flow separation, considerable recirculation regions, and the turbulent wake trailing the pantograph. The closely spaced streamlines over the pantograph reveal intense low-pressure areas, thus contributing to the rise of lift and drag. As the reference case, it is associated with a drag coefficient ( $C_d$ ) of 0.5923 and a lift coefficient ( $C_l$ ) of 0.188.

Compared to the uncovered model, Design 1 (see Figure 12) shows modest aerodynamic improvements. The airflow is smoother along the train nose; however, there are still significant disturbances around the pantograph. While vortices behind the pantograph and close to the rear increase pressure drag, streamline acceleration and bending over the pantograph produce very small areas of high-velocity and flow separation. Recirculation regions at the pantograph base also break the flow, thereby giving a drag coefficient ( $C_d$ ) of 0.3341 and a lift coefficient ( $C_l$ ) of 0.087.

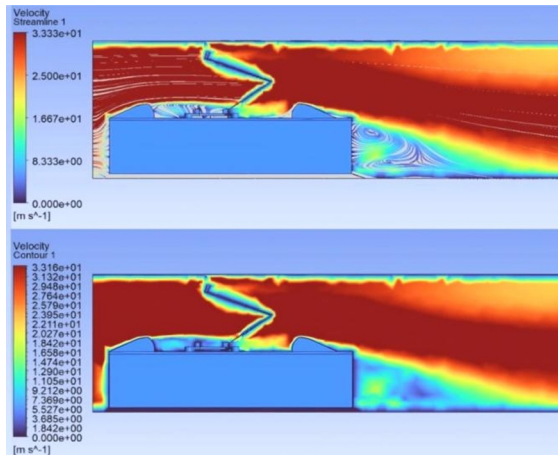


**Fig. 13.** Design 2, Fairing 35° inclined, with outward curvature at the end.

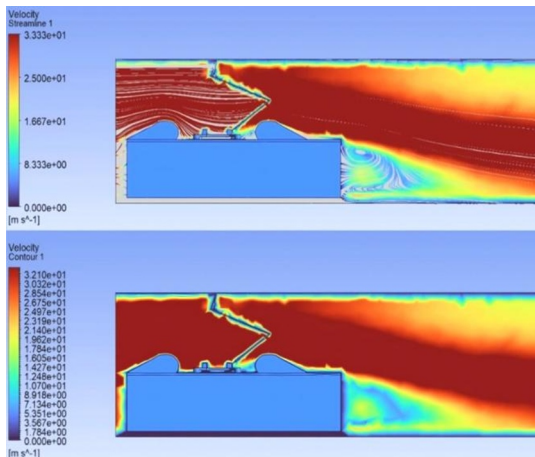


**Fig. 14.** Design 3, Fairing 35° inclined, with inward curvature at the end.

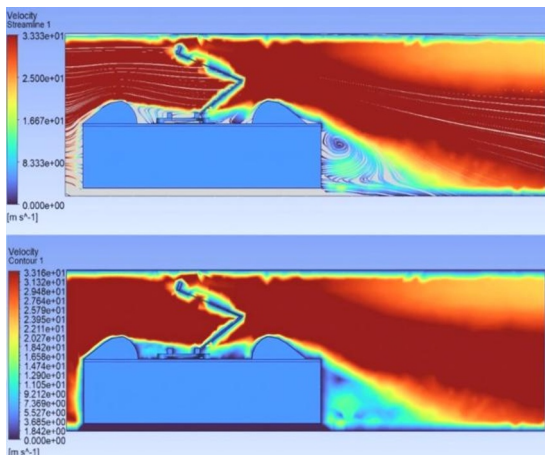


**Fig. 15.** Design 4, Fairing 45° inclined, with flat end.

As shown in Figure 13, Design 2 shows more fluid streamline patterns and a less obvious wake, thus indicating visually that the airflow is cleaner. However, the lower angle of inclination results in a poorer pressure distribution, and the larger exposed frontal area of the body increases the form drag. In spite of the fact that it looks streamlined, the aerodynamic efficiency of this design is compromised by these factors with a drag coefficient ( $C_d$ ) of 0.4210 and a lift coefficient ( $C_l$ ) of 0.084.

The best aerodynamic performance is demonstrated by Design 3 as shown in Figure 14, which has an inward-curved fairing angled at a 35° angle. Because the wake region is relatively small and the streamlines flow very smoothly with nearly no separation, vortex formation is controlled. The optimized curvature helps the pressure distribution and flow uniformity so that the lowest drag ( $C_d = 0.2881$ ) and lift ( $C_l = 0.062$ ) can be achieved from all the configurations, thus making it the most aerodynamically efficient design.

Design 4 exhibits extremely unfavorable aerodynamic behavior due to its abrupt curvature and steeper 45° slope as shown in Figure 15. Separation of the flow over the pantograph happens already in the most part thus a big wake is generated increasing pressure drag, while very sharp acceleration over the top surface leads to a big pressure differential thus lift is increased considerably. When compared to smoother, curved designs, both drag ( $C_d = 0.4421$ ) and lift ( $C_l = 0.148$ ) are higher due to the steep geometry's altered flow direction and increased vortex formation.

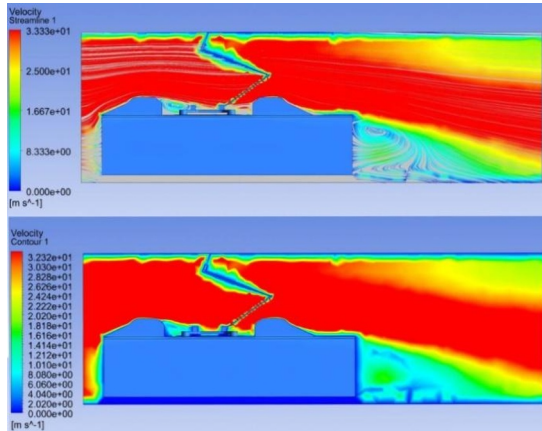


**Fig. 16.** Design 5, Step up design, Fairing 35° inclined with flat end.

As illustrated in Figure 16, Design 5 shows a moderately enhanced aerodynamic performance with more streamlined streamlines and less flow separation relative to Design 4. The wake is more streamlined, and although vortices remain, they are less powerful. The airflow is still more attached on the pantograph surface, thus a more uniform pressure distribution is ensured. Consequently, the design achieves a state of equilibrium of aerodynamic characteristics with moderate lift ( $C_l = 0.125$ ) and drag ( $C_d = 0.3105$ ), making it a stable, mid-performance configuration.

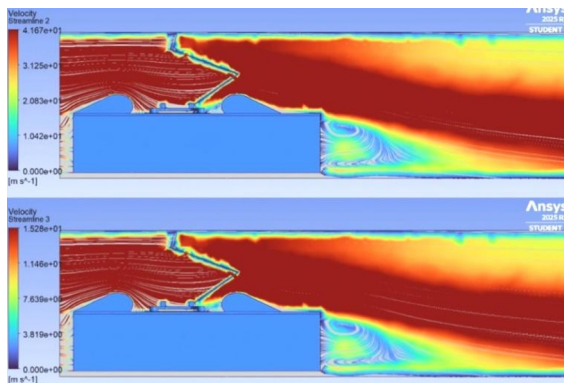


**Fig. 17.** Design 3, analysed at 150km/hr & 55km/hr respectively.

Design 3, which was also tested at 55 and 150 km/h as shown in Figure 17, consistently demonstrated greater flow aerodynamic stability. The drag ( $C_d = 0.3001$ ) and lift ( $C_l = 0.085$ ) were kept at very low levels at 150 km/h because the flow was very near to the surface with very little boundary layer separation. With a smaller wake and less drag ( $C_d = 0.2624$ ,  $C_l = 0.059$ ), the airflow surrounding the pantograph stayed laminar and stable at 55 km/h. These results lead to the conclusion that Design 3 is both effective and adaptable to varying operating speeds.

## 5. Conclusion

The present study demonstrates that the incorporation of fairings on the pantograph sinking platform significantly enhances the aerodynamic performance of the WAG-12 high-speed train car. The uncovered (baseline) configuration exhibits the highest aerodynamic drag ( $C_d = 0.5923$ ) and lift ( $C_l = 0.188$ ) due to severe flow separation, extensive recirculation zones, and a turbulent wake behind the pantograph. Among the five fairing designs evaluated, Design 3 (35° inward-curved fairing) delivers the most superior aerodynamic efficiency, achieving the lowest drag coefficient ( $C_d = 0.2881$ ) and lift coefficient ( $C_l = 0.062$ ) at 120 km/h. This design effectively minimizes flow separation, suppresses vortex formation, and produces a streamlined wake with minimal turbulence, as evidenced by smoother streamlines

and reduced low-pressure regions. Additional simulations at 55 km/h and 150 km/h further confirm Design 3's robustness and adaptability across a wide range of operating speeds, maintaining low drag and lift values with stable flow attachment. In comparison, Design 1 and Design 2 offer moderate drag reductions ( $C_d = 0.3341$  and  $0.4210$ , respectively), but suffer from residual recirculation and wake disturbances. Design 4 ( $45^\circ$  inclination) results in early flow detachment and increased drag ( $C_d = 0.4421$ ), while Design 5 (step-up configuration) provides balanced but suboptimal performance ( $C_d = 0.3105$ ,  $C_l = 0.125$ ). These findings underscore the critical role of fairing inclination angle, end curvature, and overall geometry in controlling flow separation and reducing aerodynamic forces around the pantograph. The results highlight that inward-curved fairings with optimized angles (e.g.,  $35^\circ$ ) offer the most effective solution for minimizing drag and improving aerodynamic stability in high-speed train pantograph systems. This work provides valuable aerodynamic insights for future design improvements and supports the development of energy-efficient, high-speed rail technologies with reduced environmental impact and operational costs.

## Acknowledgements

The authors extend their sincere gratitude to VIT Bhopal University for providing essential support for the simulation work. Grok AI tool was used for language refinement and improving the clarity of the manuscript. All technical content, results, and conclusions are the sole work of the authors.

## References

1. Zhang, L., Zhang, J., Li, T., & Zhang, W. Influence of pantograph fixing position on aerodynamic characteristics of high-speed trains. *Journal of Modern Transportation*, **25**(1), 34–39 (2017).
2. Zhang, L., & Yang, M. Wind tunnel experimental of impact on aerodynamic characteristics for vehicle by pantograph equipment. *Journal of Central South University (Science and Technology)*, **42**, 3894–3898 (2011).
3. Hongkang Liu, Shishang Zhang, Xifeng Liang & Yong Zou, The effect of covering structure in pantograph sinking platform on the aerodynamics of high-speed train, *Engineering Applications of Computational Fluid Mechanics*, **16**:1, 2156-2174 (2022).
4. Xiao, C.-H., Yang, M., Tan, C., & Lu, Z. Effects of platform sinking height on the unsteady aerodynamic performance of high-speed train pantograph. *Journal of Wind Engineering and Industrial Aerodynamics*, **204**, 104284 (2020).
5. Raghunathan, R. S., Kim, H. D., & Setoguchi, T. Aerodynamics of high-speed railway train. *Progress in Aerospace Sciences*, **38**(6–7), 469–514. (2002).
6. Wu, Z., Xie, Z., Wang, P., & Ding, W. Aerodynamic drag performance analysis of different types of high-speed train pantograph fairing. *Journal of Applied Science And Engineering*, **23**, 509–519. (2020).
7. Mellet C, L etourneaux F, Poisson F, Talotte C, High speed train noise emission: latest investigation of the aerodynamic/rolling noise contribution. *J Sound Vib* **293**(3–5):535–546 (2006).
8. Thompson DJ, *Railway noise and vibration: mechanisms, modelling and means of control*. Elsevier, Oxford (2008).
9. Talotte C, Aerodynamic noise: a critical survey. *J Sound Vib* **231**(3):549–562(2000).

10. Talotte C, Gautier PE, Thompson DJ, Hanson C, Identification, modelling and reduction potential of railway noise sources: a critical survey. *J Sound Vib* **267**(3):447–468 (2003).
11. Hongkang Liu, Shishang Zhang, Xifeng Liang & Yong Zou, Numerical study on the effect of pantograph fairing on aerodynamic performance at various train heights, *Engineering Applications of Computational Fluid Mechanics* **17**:1(2023).
12. WAG-12 loco pilot handbook, (Electric loco training centre, Tatanagar, 2023).
13. Government of India (Ministry of Railways), Technical specification for high-reach pantograph for AC freight electric locomotives, (Research Designs and Standards Organisation, Manak Nagar, Lucknow, 2012).
14. Devasthali, N., Linoj, K. C., Kale, M. & Sharma, R. Numerical Investigation of Isothermal Nonswirling Turbulent Jet in an Axial Plus Tangential Swirl Burner. in *International Conference on Sustainable Technologies and Advances in Automation, Aerospace and Robotics* 315–326 (2024).
15. Linoj, K. C., Devasthali, N., Kale, M. & Sharma, R. CFD Study of Isothermal Non-swirling Turbulent Jet Under Confined Conditions in an Axial-Tangential Swirl Burner Using K-Omega Turbulence Modeling. in *International Conference on Recent Advances in Mechanical Infrastructure* 385–398 (2025).